





Particulate matter flux interception in oceanic mesoscale eddies by the polychaete *Poeobius* sp.

Svenja Christiansen ^{1,a*} Henk-Jan Hoving,¹ Florian Schütte,¹ Helena Hauss,¹ Johannes Karstensen ¹, Arne Körtzinger,^{1,2} Simon-Martin Schröder,² Lars Stemmann,³ Bernd Christiansen,⁴ Marc Picheral,³ Peter Brandt ^{1,2} Bruce Robison,⁵ Reinhard Koch,² Rainer Kiko ¹

¹GEOMAR Helmholtz-Centre for Ocean Research Kiel, Kiel, Germany

²Christian-Albrechts-Universität zu Kiel, Kiel, Germany

³Sorbonne Universités, UPMC Université Paris 06, CNRS, Laboratoire d’Océanographie de Villefranche (LOV) UMR7093, Observatoire Océanologique, Villefranche-sur-Mer, France

⁴Institut für Hydrobiologie und Fischereiwissenschaft, Universität Hamburg, Hamburg, Germany

⁵Monterey Bay Aquarium Research Institute, Moss Landing, California

Abstract

Gelatinous zooplankton hold key functions in the ocean and have been shown to significantly influence the transport of organic carbon to the deep sea. We discovered a gelatinous, flux-feeding polychaete of the genus *Poeobius* in very high abundances in a mesoscale eddy in the tropical Atlantic Ocean, where it co-occurred with extremely low particle concentrations. Subsequent analysis of an extensive in situ imaging dataset revealed that *Poeobius* sp. occurred sporadically between 5°S–20°N and 16°W–46°W in the upper 1000 m. Abundances were significantly elevated and the depth distribution compressed in anticyclonic modewater eddies (ACMEs). In two ACMEs, high *Poeobius* sp. abundances were associated with strongly reduced particle concentrations and fluxes in the layers directly below the polychaete. We discuss possible reasons for the elevated abundances of *Poeobius* sp. in ACMEs and provide estimations showing that a single zooplankton species can completely intercept the downward particle flux by feeding with their mucous nets, thereby substantially altering the biogeochemical setting within the eddy.

Primary production by marine phytoplankton contributes about 50% to the global biological carbon dioxide withdrawal from the atmosphere (Field et al. 1998). This biomass

production and the subsequent active and passive export to deeper water layers and ultimately the seafloor—mostly in the form of small to large particles—is termed the biological

*Correspondence: svenja.christiansen@ibv.uio.no

Present address:

^aDepartment of Biosciences, University of Oslo, Oslo, Norway

S.C., H.-J.H., and R.K. contributed equally.

Author Contribution Statement: This study was designed by Svenja Christiansen, Rainer Kiko, and Henk-Jan Hoving. Svenja Christiansen analyzed the data in consultation with Rainer Kiko and Henk-Jan Hoving. Bernd Christiansen, Peter Brandt, Johannes Karstensen, Lars Stemmann, Helena Hauss, Arne Körtzinger, Florian Schütte, and Bruce Robison added valuable input to the further development of the study and the data interpretation. Florian Schütte identified the eddy status of all UVP5 profiles. Simon-Martin Schröder and Reinhard Koch developed the deep learning algorithms for the image classification. Marc

Picheral provided analytical tools for the UVP5 data processing. All authors contributed to writing the paper. All authors approved the final submitted manuscript.

Data Availability Statement: All UVP5 image data are available upon reasonable request on <http://ecotaxa.obs-vlfr.fr/>. UVP5 particle data and CTD data are available at <https://doi.pangaea.de/10.1594/PANGAEA.888952>.

Additional Supporting Information may be found in the online version of this article.

This is an open access article under the terms of the Creative Commons Attribution-NonCommercial License, which permits use, distribution and reproduction in any medium, provided the original work is properly cited and is not used for commercial purposes.

carbon pump (Volk and Hoffert 1985). Together with the physical and microbial (Jiao et al. 2010) carbon pump, the biological carbon pump plays a major role in the natural carbon cycle and the oceanic climate buffering system (Sabine and Tanhua 2010; Heinze et al. 2015). A mechanistic understanding of the processes that are regulating the biological carbon sequestration is required to predict and model the biological carbon pump on local to global scales.

The efficiency of the biological carbon pump varies strongly and depends particularly on plankton community dynamics and processes (e.g., Legendre and Rivkin 2002; Cavan et al. 2017). Zooplankton contribute to the biological carbon pump by producing fast-sinking particles in the form of fecal pellets (Wilson et al. 2013) and dead bodies (Frangoulis et al. 2011). Furthermore, many species contribute substantially to the active transport of carbon to depth by performing diel vertical migrations (Riley 1951; reviewed by Packard and Gómez 2013); they feed at the surface at night and migrate to depth during the day, where respiration (Bianchi et al. 2013), excretion (Steinberg et al. 2008), defecation (Angel 1984), predation, and other metabolic processes (e.g., Longhurst et al. 1990) continue to take place.

Part of the sinking particulate organic matter is consumed by deeper-living zooplankton, particularly by filter feeders and flux feeders. Filter feeders such as salps (Hamner et al. 1975) and different copepod species (Kjørboe 2000) retrieve particulate matter from a continuous flow of water generated through their feeding apparatus. Pteropods and some polychaetes (Hamner et al. 1975; Jackson 1993; Uttal and Buck 1996; Stemmann et al. 2004; Turner 2015) deploy net-like mucous structures on which they collect sinking particles; this feeding mode is termed flux-feeding (Jackson 1993).

Flux-feeding has been hypothesized to contribute strongly to particulate matter loss processes in the upper ocean. Iversen et al. (2010) compared in situ particle profiles with shipboard measurements of particle sinking velocities and respiration rates off Cape Blanc. The authors concluded that microbial respiration alone could not explain the observed organic matter degradation but that instead, zooplankton flux-feeding was the dominant degradation process in the upper water column. Pteropods are flux-feeders that use mucous nets of several times their own body size to catch sinking particles from the water column (Gilmer 1972). Jackson (1993) assessed the influence of these animals' mucous nets on vertical particle flux and found a median flux reduction of 26% by two species alone in the upper 100 m of five different regions in the Atlantic Ocean. Observations with remotely operated vehicles in the Pacific Ocean have shown that the flux-feeding polychaete *Poeobius meseres* significantly reduces the concentration of very small particles (transmissometer data) in the deep sea (Robison et al. 2010).

Enhanced zooplankton (Ring 1981; Tsurumi et al. 2005; Stemmann et al. 2008; Godø et al. 2012; Hauss et al. 2016) and particle abundances (Sweeney et al. 2003; Fiedler et al.

2016; Waite et al. 2016) within mesoscale eddies suggest particularly dynamic zooplankton-particle interactions in these ecosystems. Indeed, Goldthwait and Steinberg (2008) found increased zooplankton fecal pellet flux in mesoscale eddies in the Sargasso Sea during periods of enhanced zooplankton abundances in the surface layer, compared with the surrounding open ocean. However, the interaction between zooplankton and mesoscale eddy biogeochemistry is still poorly understood and remains an important topic in marine ecology.

Mesoscale eddies are features of rotating water masses with diameters reaching about 100 km in the eastern tropical North Atlantic (Chelton et al. 2011). Three eddy types are distinguished (Schütte et al. 2016b): anticyclones (ACs), cyclones (CEs), and anticyclonic mode-water eddies (ACMEs; McGillicuddy et al. 2007; Schütte et al. 2016b). Considering local productivity, ACs are generally low productive features, while CEs and ACMEs are generally perceived as “oases” of elevated productivity in oligotrophic open ocean environments (McGillicuddy et al. 2007; Godø et al. 2012; Hauss et al. 2016). While the rotating waterbody and the water stratification lead to the isolation of the water mass within the eddy (hereafter called the eddy core; Karstensen et al. 2017), dynamic processes that are operating at the sub-mesoscale (1–10 km) are responsible for upward nutrient supply into the euphotic zones of these eddies (Lévy et al. 2012; d'Ovidio et al. 2013; Karstensen et al. 2017). This triggers enhancement of primary production (Sweeney et al. 2003; Stramma et al. 2013; Löscher et al. 2015), zooplankton, nekton (Godø et al. 2012; Hauss et al. 2016) and particle abundance (Sweeney et al. 2003; Fiedler et al. 2016; Waite et al. 2016) as well as oxygen consumption, which may lead to suboxic, and eventually even anoxic conditions in the eddy cores (Karstensen et al. 2015; Fiedler et al. 2016; Hauss et al. 2016; Schütte et al. 2016a; Waite et al. 2016). Beneficial environmental conditions might create a niche for specific zooplankton organisms (Godø et al. 2012; Hauss et al. 2016), but whether zooplankton aggregations mainly result from migration of specimens from the eddy periphery into the eddy core, or from altered reproduction success and mortality remains an important question.

Our deployments of a pelagic in situ observation system (PELAGIOS, Hoving et al. unpubl.) in the tropical Atlantic led to the discovery of an undescribed species of the fragile polychaete genus *Poeobius* (Fig. 1a). Within one particular ACME, *Poeobius* sp. was exceptionally abundant and seemed to impact the particle abundance. This is the first record of this genus in the Atlantic Ocean while in the Pacific Ocean, the congener *P. meseres* (Heath 1930) is fairly well known from both net catches and remotely operated vehicle observations (McGowan 1959; Uttal and Buck 1996; Robison et al. 2010). *P. meseres* is a gelatinous, holoplanktonic polychaete that reaches lengths of up to 2.7 cm (Robbins 1965). In Monterey Bay, *P. meseres* has a bimodal depth distribution,

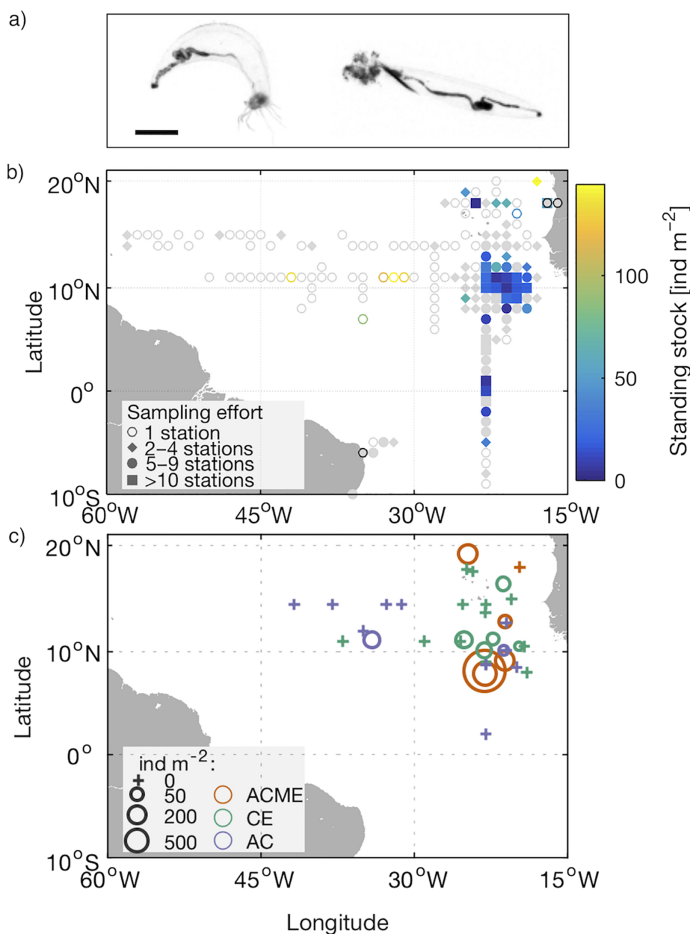


Fig. 1. Examples and distribution of *Poeobius* sp. in the tropical Atlantic Ocean. (a) Two *Poeobius* sp. specimens as recorded by the UVP5. The scale bar is 5 mm. (b) Horizontal distribution in 1-degree gridded non-eddy conditions. Gray symbols indicate that no *Poeobius* sp. was recorded, symbols with a black border indicate shelf stations with less than 600 m water depth. (c) *Poeobius* sp. standing stocks (0–600 m) in all identified eddies with ACME = anticyclonic modewater eddy, CE = cyclone, and AC = anticyclone.

with highest abundances between 300–500 m and 1600–2200 m depth (*P. meseres* (Heath, 1930). Deep-Sea Guide (DSG) at <http://dsg.mbari.org/dsg/view/concept/Poeobius%20meseres>. Monterey Bay Aquarium Research Institute (MBARI). Consulted on 2 May 2018). The polychaete feeds on detritus by deploying a free-floating mucous net or by catching particles with its tentacles (Uttal and Buck 1996).

The discovery of *Poeobius* sp. on PELAGIOS video recordings enabled the identification of this polychaete also on quantitative Underwater Vision Profiler (UVP5; Picheral et al. 2010) image data. To characterize the *Poeobius* sp. distribution we analyzed a dataset of 956 vertical UVP5 profiles obtained in the tropical Atlantic in the years 2012–2015. Using satellite, conductivity-temperature-depth (CTD), and shipboard Acoustic Doppler Current Profiler (ADCP) data, we categorized each UVP5 station to be either non-eddy, CE,

AC, or ACME. This enabled us to assess the abundance and potential biogeochemical impact of *Poeobius* sp. in these different environments and to estimate the potential effects of these organisms on particle export.

Material and methods

We analyzed a dataset of 1.82 million UVP5 images from 956 vertical UVP5 deployments that were conducted during 13 cruises in the tropical North Atlantic between 16°W to 46°W and 5°S to 20°N (Fig. 1b) in the years 2012–2015. Environmental data (temperature, salinity, and oxygen concentration) were obtained from concurrent CTD deployments. A total of 956 vertical profiles were taken at 719 stations (station defined as all profiles within 0.01° and sampled within less than 7 d). Of all profiles analyzed, 821 UVP5 profiles were conducted down to at least 600 m depth, 722 profiles down to at least 1000 m depth, and 260 profiles down to at least 3000 m depth. A total of 42 profiles were sampled at African and 9 profiles at Brazilian coastal stations (water depths < 600 m).

Assignment of profiles to eddies

We differentiated between CEs, ACs, and anticyclonic modewater eddies (ACMEs; Schütte et al. 2016b). CEs are defined by a cyclonic rotation corresponding to a negative sea level anomaly and by lower sea surface temperature and sea surface salinity than in the surrounding ocean. ACs and ACMEs both feature anticyclonic rotation and a positive sea level anomaly but differ in their density structure and therefore also in their sea surface temperature and sea surface salinity: While ACs have higher sea surface temperature and sea surface salinity, ACMEs can be identified by cold and more saline surface signatures (Schütte et al. 2016b). These physical characteristics are usually associated with high productivity in CEs and ACMEs. Therefore, these eddies can also be identified by high Chlorophyll a levels and a shallow oxygen minimum zone at the base of the photic layer around 50–100 m depth (thereby distinguished from the midwater oxygen minimum zone, which can usually be found between 300 m and 700 m depth in the eastern tropical North Atlantic; Brandt et al. 2015; Schütte et al. 2016b). Several mesoscale eddies were already identified during the respective cruises (Supporting Information Table S1) due to their distinct vertical oxygen profiles and velocity structure (swirl velocity around the eddy core). The profiles which were located in those eddies were assigned to the respective eddy category. The eddy status of all other profiles was determined by automatic identification using satellite images and subsequent validation with CTD and ADCP data as described in Schütte et al. (2016b). The applied algorithms detected eddies with a radius > 45 km. The coarse resolution of the satellite data (0.25° × 0.25°) leads to an increasing probability to include profiles from outside the eddy with increasing distance from the eddy core. Therefore, in order to avoid the inclusion of profiles taken at the margins or outside of

eddies, only profiles that were located within 40 km distance of an eddy center were assigned to the respective eddy type. This may have led to an underestimation of eddy profiles. See Supporting Information Table S1 for information on deployments in eddy conditions. Profiles that were recorded within the same eddy were averaged before the comparative analysis of the different eddy types and background conditions was performed.

UVP5 measurements

The UVP5 was mounted on the CTD rosette frame and deployed vertically. During a cast, the instrument takes between 6 images per second and 11 images per second of a defined volume (Picheral et al. 2010). In this study, we used three different UVP5 (serial numbers sn000, sn001, and sn010) which recorded volumes of 0.95 L, 0.93 L, and 0.88 L per image, respectively. UVP5 sn000 and sn010 were calibrated against UVP5 sn001. For further information regarding the calibration process, see Picheral et al. (2010).

The UVP5 provides a quantitative method to assess abundances of particles and zooplankton, but bias may be introduced at the lower size range (due to insufficient resolution and light diffusion) and at the upper size limit due to the then comparably small sampling volume that may over- or underestimate rare organisms and particles. The UVP5 used in this study had pixel sizes of 0.151 mm (sn001 and sn010) and 0.174 mm (sn000) enabling a quantitative assessment of particles with an equivalent spherical diameter (ESD, mm) > 0.15 mm and 0.17 mm, respectively. In the following, we only use particles with ESD between 0.17 mm and 16.88 mm in logarithmic size classes for the quantitative analysis of particle abundances. Objects with an ESD > 500 μm are saved as images, so-called vignettes, and can be used for the quantification and identification of larger detritus and zooplankton, such as *Poeobius* sp. (see, e.g., Fig. 1a and Supporting Information Fig. S1).

Poeobius sp. standing stocks

Poeobius sp. vignettes were combined with previously obtained and categorized UVP5 image data to train a deep convolutional neural network (CNN) for image recognition using the Caffe framework (Jia et al. 2014). The CNN computes a discrete probability distribution over all previously defined classes and the most likely category is selected (LeCun et al. 2015). All images of the vertical UVP5 profiles obtained in the tropical Atlantic were classified using the neural network. The *Poeobius* sp. category, but also categories that were identified to contain wrongly assigned *Poeobius* sp., in total around 370,000 images, were manually validated to reduce the number of false positives (objects that were wrongly classified as *Poeobius* sp.) and false negatives (*Poeobius* sp. objects that were sorted into a different category). Identified zooplankton and artifacts were subtracted from the total particle spectrum for the presentation of vertical particle abundance profiles. *Poeobius* sp. abundance (ind

m^{-3}) was obtained within 5 m depth bins by dividing the number of individuals by the sampling volume of the respective bin. Standing stocks (ind m^{-2}) were calculated by multiplying the abundance within each depth bin with the bin size (i.e., 5 m) and integrating the standing stocks of the individual bins over the water column.

Detailed analysis of two ACMEs with particularly high *Poeobius* sp. abundance

We found particularly high *Poeobius* sp. standing stocks in two ACMEs which we hereafter refer to as ACME1 and ACME2. For these two eddies, we performed a more detailed analysis in order to explore the potential causes and consequences of the high *Poeobius* sp. abundances. We compared the conditions that we observed in ACME1 and ACME2 with data from 12 background profiles that were obtained at the same location as the eddies but during non-eddy conditions. Background data included validated profiles of the cruises M97, MSM22, M105, M106, and PS88b.

Determination of stratification

Water column stratification can occur where strong density gradients exist and may increase particle retention (MacIntyre et al. 1995; Kindler et al. 2010). We calculated the potential density (σ_θ , kg m^{-3}) and the squared buoyancy frequency (Brunt-Väisälä frequency N^2 , s^{-2}), which gives an indication of the change in density with depth, using the Gibbs-SeaWater (GSW) Oceanographic toolbox (Version 3.05 for MATLAB) that is based on the TEOS-10 convention (McDougall and Barker 2015).

Poeobius sp. size and biomass

Length and width of all recorded *Poeobius* sp. were measured manually on the individual UVP5 images with *ImageJ* (<http://www.imagej.net>). The measured length and width was used to calculate the individual area (Area, mm^2), estimated as prolate ellipse, of all recorded *Poeobius* sp. Biomass in terms of dry weight (DW, μg) was determined from this area, using the relation by Lehette and Hernández-León (2009) for gelatinous zooplankton (siphonophores):

$$\text{DW} = 43.17 \times \text{Area}^{1.02} \quad (1)$$

Vertical biomass profiles for ACME1 and ACME2 were calculated from the individual lengths, widths, and abundances of *Poeobius* sp. for each 5 m depth bin.

Other zooplankton

Poeobius sp. abundance in relation to other zooplankton was assessed in ACME1, ACME2, and in the background profiles. In addition to *Poeobius* sp., three categories of zooplankton were differentiated: copepods, Rhizaria (as classified in Biard et al. 2016) and “other zooplankton” (containing all other identified zooplankton groups, e.g., non-copepod crustaceans, medusa, etc.). Additionally, *Poeobius* sp. and macrozooplankton were counted on a 15 min 11 s pelagic video

transect at 110 m depth that was recorded with PELAGIOS in ACME2. *Poeobius* sp. and macrozooplankton counts in that transect were estimated by selecting six sections (9–13 s length each) of the transect where the camera was towed steadily. In these sections, the number of *Poeobius* sp. and several other macrozooplankton groups were counted, resulting in an abundance per second estimate for these groups for each section. The values of all six sections were averaged and multiplied by the length of the total transect. This process was repeated three times and the mean calculated. No PELAGIOS data were available from ACME1.

Particle size distribution

We compared the particle abundance spectra of ACME1 and ACME2 with those of the 12 background profiles. For this purpose, we defined two 10 m depth intervals, one above and one below the layer where *Poeobius* sp. occurred. The particle abundance of each layer was plotted against the particle size on a double logarithmic scale. The slope of the resulting log-log linear relationship between particle abundance and size was calculated for each depth layer in ACME1, ACME2, and the respective background data.

Detritus flux

Detritus flux was calculated from the abundance and size of particles in individual size classes, thus using the particle abundance measured by the UVP5 as a proxy for vertical flux. Only particles identified as detritus (including fecal pellets) on the UVP5 vignettes, were included in the analysis. First, the carbon content (m_{insitu} , mmol C) of the detritus in the different size classes was calculated:

$$m_{\text{insitu}} = a \times \text{ESD}^b \times R \quad (2)$$

with the constants $a = 273$ and $b = 1.62$ (Kriest 2002), ESD = equivalent spherical diameter (cm) and $R = 106/16$ (Redfield stoichiometry; Redfield et al. 1963). We used the equation for miscellaneous aggregates (Allredge 1998).

Then, sinking velocities (sink_{k2002} , m d^{-1}) of individual detritus particles in the different size classes were calculated:

$$\text{sink}_{k2002} = c \times \text{ESD}^d \quad (3)$$

with the constants $c = 132$ and $d = 0.62$ (Kriest 2002). Finally, for each size class, the flux (F , $\text{mg C m}^{-2} \text{d}^{-1}$) of a single detritus particle was calculated from the particles sinking velocity, sink_{k2002} , and its carbon content, m_{insitu} .

$$F = \text{sink}_{k2002} \times m_{\text{insitu}} \times M_C \quad (4)$$

with $M_C = 12 \text{ g mol}^{-1}$ (molar mass of carbon).

Individual detritus particle masses and detritus fluxes of each size class were multiplied with the particle abundance in the respective 5 m depth bin. Detritus mass and flux were integrated for the size classes 0.5–16.88 mm in order to obtain the total detritus mass flux of this size range. Our calculations

exclude zooplankton, but also neglect the role of smaller detritus ($< 500 \mu\text{m}$ ESD) and thus are not representative for the total particle flux. Furthermore, our flux calculations are based on global relationships between aggregate size and sinking velocities (Kriest 2002) which can only serve to provide a first-order estimate of the actual flux, as local variations in these relationships might occur (McDonnell and Buesseler 2012). Therefore, we would like to point out that our detritus flux estimates mainly serve to compare between ACME and background conditions.

Microbial particle-associated respiration rates

Microbial particle-associated respiration rates (PARR, $\mu\text{mol kg}^{-1} \text{yr}^{-1}$) for particles between 0.17 mm and 16.88 mm ESD were calculated as a function of particle size (ESD, mm), ambient temperature, and oxygen concentration as done by Kalvelage et al. (2015). These PARR are based on empirical relationships between aggregate diameter and respiration rate that were measured by Iversen et al. (2010) and corrected for the occurrence of anoxic conditions inside the aggregate according to Ploug et al. (1997). The PARR of individual size classes were integrated by particle abundances in the different size classes. PARR estimates at 100–600 m depth in 12 background profiles coincide well with apparent oxygen utilization rate estimates that range between $2 \mu\text{mol kg}^{-1} \text{yr}^{-1}$ and $12 \mu\text{mol kg}^{-1} \text{yr}^{-1}$ for the tropical Atlantic Ocean below 100 m depth (Karstensen et al. 2008).

Poeobius sp. respiration

Poeobius sp. respiration (R_{poeo} , $\mu\text{mol ind}^{-1} \text{h}^{-1}$) was calculated based on the specific respiration rate (R_{Th}) of $0.068 \mu\text{mol g}^{-1}$ (wet weight) h^{-1} that was measured by Thuesen and Childress (1993) for the Pacific Ocean congener *P. meseres*. A Q_{10} temperature coefficient of 2 was applied considering the experimental temperature of 5°C in Thuesen and Childress (1993) and temperatures of around 15°C in the ACME cores. An assumed body shape of a prolate ellipse with mean seawater density (ρ , 1.023 g mL^{-1}) served to define the wet weight (WW_{poeo}) of a *Poeobius* sp. of a certain length l and width w .

$$\text{WW}_{\text{poeo}} = \left(\left(\frac{4 * \text{pi}}{3} \right) \times \left(\frac{w}{2} \right)^2 \times \left(\frac{l}{2} \right) \right) \times \rho \quad (5)$$

$$R_{\text{poeo}} = R_{\text{Th}} \times Q_{10} \times \text{WW}_{\text{poeo}} \quad (6)$$

R_{poeo} was calculated from individual body lengths in ACME1 and ACME2 and integrated for each 5 m depth bin. Respiration in $\mu\text{mol kg}^{-1} \text{yr}^{-1}$ was obtained by dividing the integrated R_{poeo} by the volume recorded in the respective depth bin, multiplying with 8760 to get to values per year and dividing by mean seawater density (1023 kg m^{-3}).

Poeobius sp. flux interception potential

We identified *Poeobius* sp. mucous nets from PELAGIOS HD video recordings by running the video in slow mode and

identifying patches of particles that were attached to a *Poeobius* sp. and moved in the same way through the cameras field of view (see Supporting Information Video S1). The area of the mucous nets was estimated based on frame shots from the video. As the field of view of PELAGIOS is unknown and objects cannot be scaled absolutely, the net size was determined relative to the size of the *Poeobius* sp. specimen attached to it. Relative length, width, and area of nets on five frame shots were measured manually in *ImageJ* (Supporting Information Fig. S2). Additionally, the net area was approximated as a prolate ellipse from the net length and width that was measured relative to *Poeobius* sp. length. Considering that the aspect of the towed camera system was from the side, not from above/below (which is likely the maximum net surface area to optimize sinking particle capture), our size estimations have to be considered as cautious approximations and are likely underestimates.

The potential total area covered by all *Poeobius* sp. mucous nets A_{total} at a given station was calculated as:

$$A_{\text{total}} = St_{\text{di}} \times p_{\text{feeding}} \times A_{\text{net}} \quad (7)$$

where St_{di} is the standing stock (ind m^{-2}) in the defined depth interval where *Poeobius* sp. occurred, p_{feeding} is the proportion of nets deployed, and A_{net} is the mean net area (m^2) as determined from the mean length of the *Poeobius* sp. in the respective eddy and the relations described above.

Statistics

Data visualization was done in MATLAB R2016b. All statistical tests were done in the R statistical environment. To account for non-normal distributions and unequal sample sizes, the following non-parametric statistical tests were applied:

1. The Mann-Whitney U test (R-function *wilcox.test*, *stats* package) was used for comparing *Poeobius* sp. standing stocks between non-eddy stations and stations of different eddy types.
2. The two-sample Kolmogorov-Smirnov test (R-function *ks.test*, *stats* package) was used for comparing the distribution of depth occurrences between non-eddy stations and stations of different eddy types.
3. Confidence intervals (95%) were used to present the variation of the 12 background profiles that were sampled at the same location as the two eddies with highest *Poeobius* sp. standing stocks (ACME1 and ACME2). A statistically significant difference between these background conditions and the ACME was assumed when the ACME values were outside the 95% confidence interval.

Only data from the upper 600 m were considered for comparing both standing stocks and depth distribution.

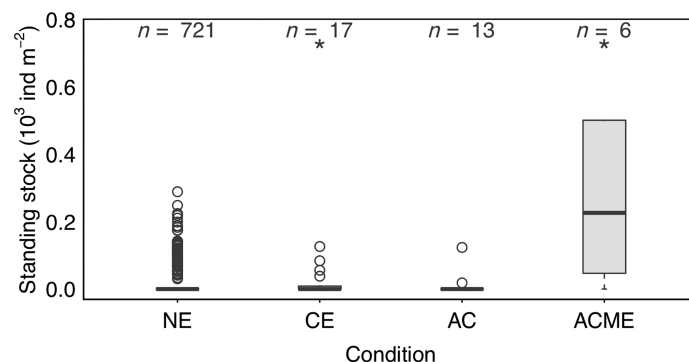


Fig. 2. *Poeobius* sp. standing stocks in non-eddy (NE) and different eddy conditions. AC, anticyclone; ACME, anticyclonic modewater eddy; CE, cyclone. Boxes represent the first and third quartile, circles are outliers. n is the number of stations for NE conditions and for different eddies. Significance of difference to non-eddy conditions with $*p < 0.05$. Only data from the upper 600 m are considered. One outlier (5523 ind m^{-2}) in ACME conditions (ACME1) is not shown here but was included in the analysis.

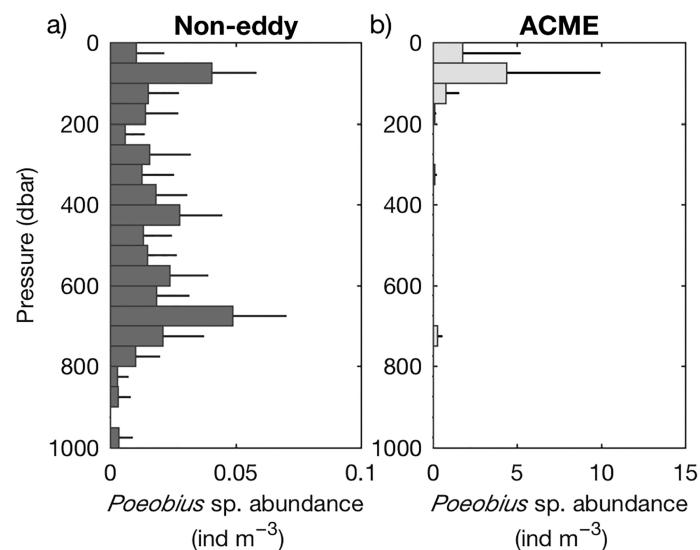


Fig. 3. Depth distribution of *Poeobius* sp. in non-eddy conditions (a) and in ACMEs (b). Data are averaged for 50 m depth bins and the positive standard deviation indicated. Please note the 50-fold larger values on the x-axis of (b). Only oceanic profiles deeper 600 m water depth are considered.

Results

Poeobius sp. was found throughout the entire observation area, except for the African or Brazilian coast (water depths < 600 m). Most identifications stem from the Guinea Dome region where the sampling effort was highest (Fig. 1b). In open ocean non-eddy profiles, all *Poeobius* sp. occurred at particle concentrations between 1 particle L^{-1} and 25 particles L^{-1} . Although 70% of the casts were deeper than 1000 m depth, *Poeobius* sp. was not observed below 1000 m, where the median particle abundance was less than

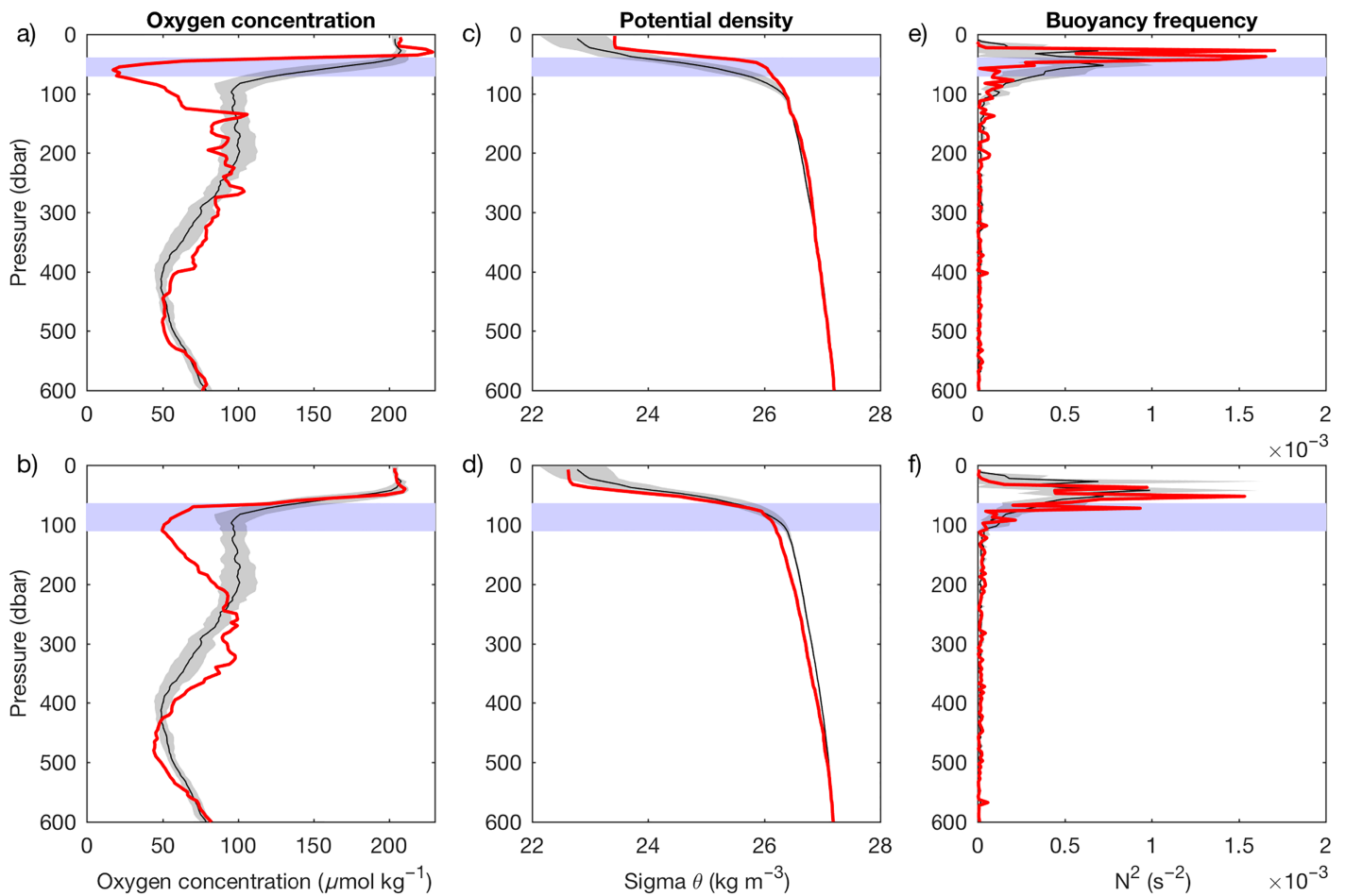


Fig. 4. Environmental characteristics of the anticyclonic modewater eddies ACME1 and ACME2. Oxygen concentration (**a**, **b**), potential density (**c**, **d**), and squared buoyancy frequency (**e**, **f**) in ACME1 (**a**, **c**, **e**) and ACME2 (**b**, **d**, **f**) compared to background (i.e., mean reference) conditions during five other cruises (12 profiles) at the same location. Red lines indicate mean eddy conditions, black lines mean reference conditions. The gray area shows the 95% confidence interval of the reference conditions. The blue shaded area indicates in which depth interval *Poeobius* sp. occurred in ACME1 and ACME2.

2 particles L^{-1} . *Poeobius* sp. was present at oxygen concentrations below the suboxic level ($< 4.5 \mu\text{mol kg}^{-1}$), as observed in one ACME (Supporting Information Fig. S3).

Observations from the upper 600 m were used to statistically compare *Poeobius* sp. standing stocks and depth distributions. *Poeobius* sp. standing stocks were significantly (Mann-Whitney U : $p < 0.05$) larger in ACMEs (median 226 ind m^{-2} , range $0\text{--}5523 \text{ ind m}^{-2}$, $n = 6$ eddies) compared to non-eddy stations (median 0 ind m^{-2} , range $0\text{--}289 \text{ ind m}^{-2}$, $n = 721$ stations, Figs. 1c, 2). The distribution of standing stocks in CEs differed significantly from non-eddy stations but the effect size was small (median in CEs 0 ind m^{-2} , range $0\text{--}126 \text{ ind m}^{-2}$, $n = 17$ eddies). No significant difference was found between ACs (median 0 ind m^{-2} , range $0\text{--}123 \text{ ind m}^{-2}$, $n = 13$ eddies) and non-eddy stations (Mann-Whitney U : $p > 0.05$).

A very shallow and narrow depth distribution was observed in ACMEs compared to the non-eddy situation

(Fig. 3). The median depth of *Poeobius* sp. at non-eddy stations was 422 m (range 32–998 m, 82 individuals, 668 profiles down to at least 1000 m depth). In ACMEs, the depth distribution differed significantly from the non-eddy depth distribution (Kolmogorov-Smirnov test (KS): $p < 0.05$) with the median depth of occurrence at 87 m (range 37–722 m, 104 individuals, 12 profiles down to at least 600 m and 6 profiles down to at least 1000 m depth). Only seven and two individuals (depth ranges 23–813 m and 253–408 m), respectively, were recorded in CEs and ACs; therefore, a detailed analysis of the depth distribution for these eddy types was not possible.

Characteristics of two ACMEs with high *Poeobius* sp. standing stocks

Two ACMEs showed especially high *Poeobius* sp. and reduced particle abundances. Both were sampled at 8°N , 23°W , one on the 22nd May 2015 (ACME1) and the other on

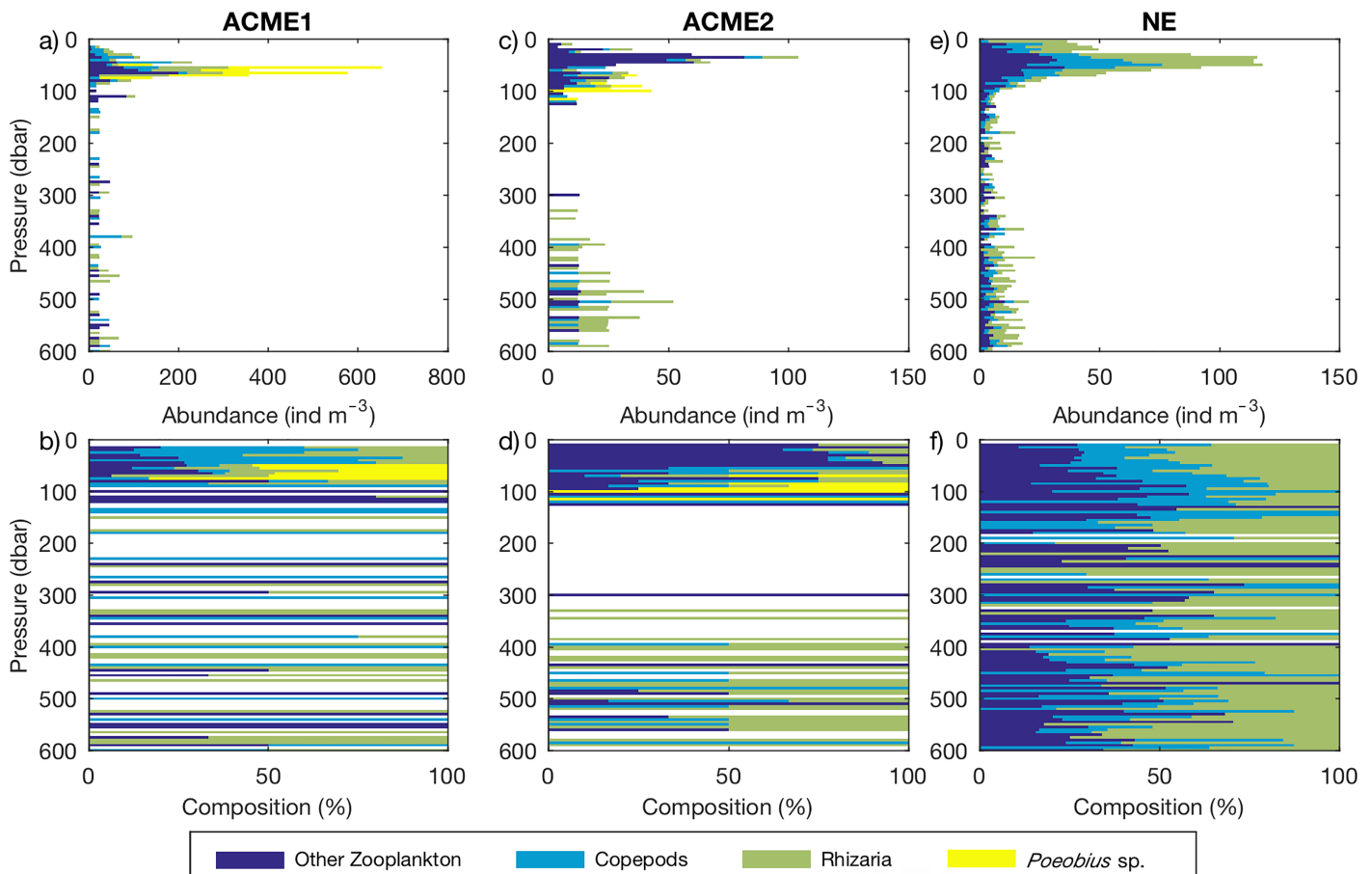


Fig. 5. Zooplankton abundance and composition in the anticyclonic modewater eddies ACME1 (a, b) and ACME2 (c, d) and in non-eddy profiles at 8°N 23°W (NE; e, f). Note the difference in scale in (a). The category “other zooplankton” includes all zooplankton not identified as either Copepod, Rhizaria, or *Poeobius* sp. and includes for example non-copepod crustaceans and jellyfish.

the 27th September 2015 (ACME2). Please see the video clips in the Supporting Information for an impression of the conditions in ACME2 (Supporting Information Video S2) compared to non-eddy conditions (Supporting Information Video S3). *Poeobius* sp. standing stock in the upper 600 m was calculated as 5523 ind m⁻² in ACME1 and as 500 ind m⁻² in ACME2. The average body length of *Poeobius* sp. was 6.7 mm (range 2.9–12.8 mm; standard deviation 2 mm, $n = 63$ individuals) in ACME1 and 14 mm in ACME2 (range 10.9–15.2 mm; standard deviation 2.1 mm, $n = 14$ individuals). For detailed *Poeobius* sp. length information, see Supporting Information Fig. S4. *Poeobius* sp. was observed between 45 m and 75 m in ACME1 and between 65 m and 115 m in ACME2, coinciding with the location of the eddy core, which is indicated by the shallow oxygen minimum zone (Fig. 4a,b). Minimum oxygen values of 17 $\mu\text{mol kg}^{-1}$ in ACME1 and 50 $\mu\text{mol kg}^{-1}$ in ACME2 were observed in this shallow oxygen minimum zone, compared to a mean minimum oxygen concentration of about 100 $\mu\text{mol kg}^{-1}$ at similar depths in background conditions observed during five cruises (12 profiles) at the same location (Fig. 4a,b).

In ACME1, the pycnocline was located at around 30 m depth, in ACME2 at around 40 m depth (Fig. 4c,d). The slope of the pycnocline appeared to be shallower in both ACMEs compared to the background conditions, which indicates a stronger stratification in the eddies. This can also be seen in the squared buoyancy frequency, which showed increased peaks of density discontinuity at the pycnocline of the two ACMEs and partly decreased values below, compared to the background profiles (Fig. 4e,f).

In the core of ACME1 and ACME2, *Poeobius* sp. constituted about 50% of the zooplankton community abundance assessed with the UVP5 (median 56%, range 35–75% over six depth intervals in ACME1 and median 44%, range 25–100% in six depth intervals where they occurred in ACME2; Fig. 5). It was absent from the zooplankton community in five non-eddy profiles sampled at 8°N 23°W during three other cruises. In one PELAGIOS video transect (15 min and 11 s, tow speed ~ 0.5 m per second) in ACME2 at 110 m, a total number of 4817 *Poeobius* sp. individuals were estimated. Only 114 other macrozooplankton organisms (65 krill, 16 fish, 12 large siphonophores [*Praya* sp.], 4 other siphonophores, 6 sergestid

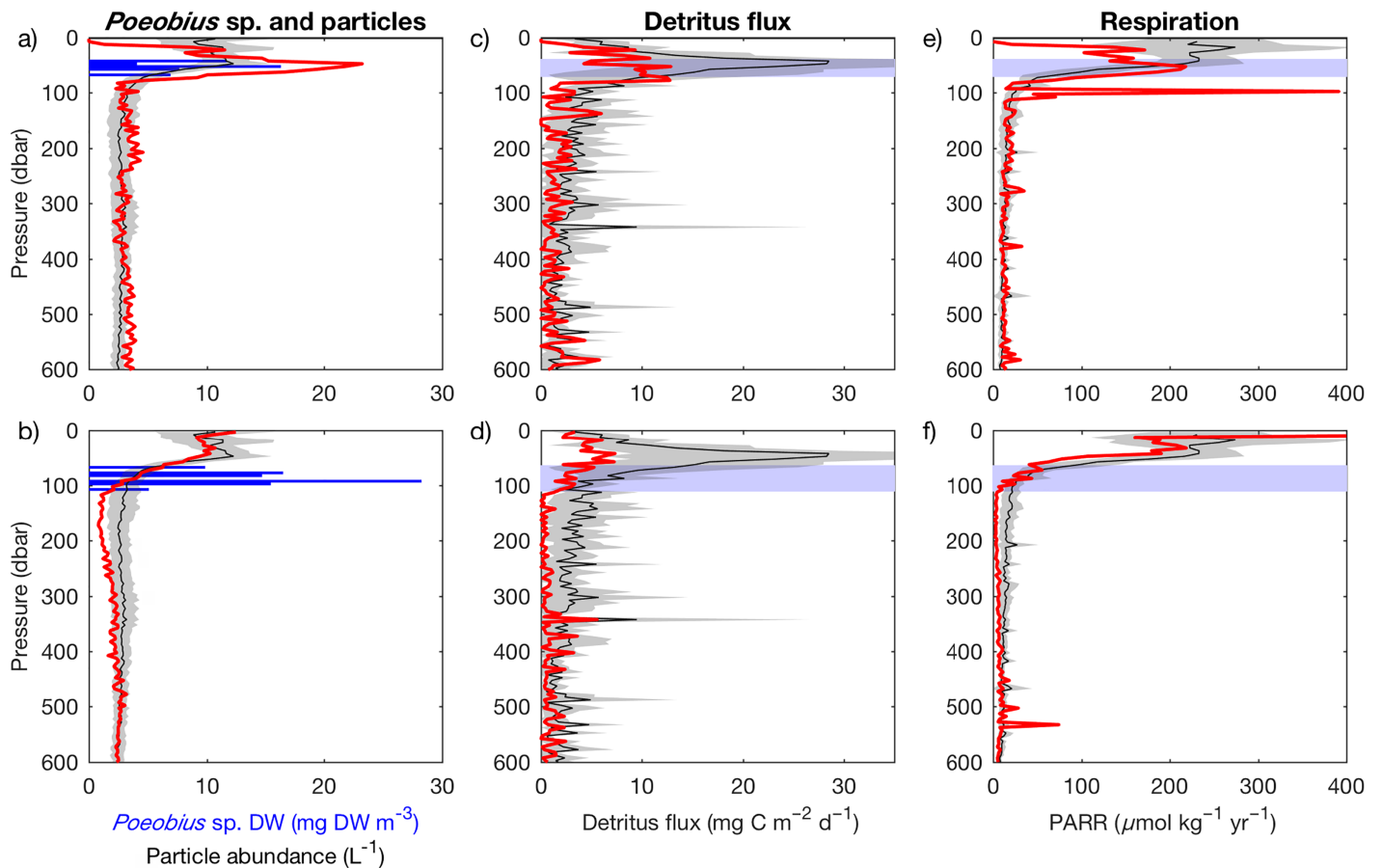


Fig. 6. *Poeobius* sp. and biogeochemical properties in the anticyclonic modewater eddies ACME1 and ACME2. *Poeobius* sp. biomass (dry weight, blue bars) and particle abundance (a, b), detritus flux (c, d) and microbial particle associated respiration rate (PARR; e, f) in ACME1 (a, c, e) and ACME2 (b, d, f) compared to background (i.e., mean reference) conditions as observed during five other cruises (12 profiles) at the same location. Red lines indicate mean eddy conditions, black lines mean reference conditions. The gray area shows the 95% confidence interval of the reference conditions. The blue shaded area in (c–e) indicates in which depth interval *Poeobius* sp. occurred in ACME1 and ACME2.

shrimps, 5 medusae, 4 ctenophores, 1 other crustacean, 1 unidentified, no salps, no appendicularians) were counted in the whole transect.

The highest *Poeobius* sp. biomass observed in ACME1 (16 mg DW m⁻³) co-occurred with the particle maximum and subsequent particle decrease in this eddy. In ACME2, high *Poeobius* sp. biomass was found below the particle maximum, but above the upper limit of the layer with less than 1 particle L⁻¹ (Fig. 6a,b). Compared to background conditions (mean particle abundance maximum of 12 particles L⁻¹), particle abundances in ACME1 (maximum of 23 particles L⁻¹) were significantly elevated—outside the 95% confidence interval of the background profiles—between 45 m and 80 m depth (Fig. 6a). The particle abundance above 40 m depth was reduced or similar to background conditions while between 80 m and 600 m abundances were usually within the background confidence interval but sometimes slightly elevated. In ACME2, on the other hand, particles were significantly depleted between 100 m and 300 m depth, with

minimum values between 110 m and 210 m depth (less than 1 particle L⁻¹, minimum 0.48 particles L⁻¹, Fig. 6b). Above 100 m and below 300 m depth, ACME2 particle abundances were within the 95% confidence interval of the background profiles.

The downward detritus flux in ACME1 was within the confidence interval of the background profiles, with a comparatively low subsurface peak flux (13 mg C m⁻² d⁻¹) compared to 44 mg C m⁻² d⁻¹ in the mean background profile (Fig. 6c). In ACME2, the downward detritus flux (subsurface peak flux of 9 mg C m⁻² d⁻¹; Fig. 6d) was almost always lower than the background flux and outside of the confidence interval. Below 100 m depth, the downward flux in ACME2 (generally below 1 mg C m⁻² d⁻¹, below 0.5 mg C m⁻² d⁻¹ between 115 m and 250 m) was significantly lower than in the background conditions (around 2.5 mg C m⁻² d⁻¹).

The PARR in the upper 50 m of ACME1 (mean of about 114 μmol kg⁻¹ yr⁻¹) was significantly reduced compared to background conditions (mean of about 234 μmol kg⁻¹ yr⁻¹;

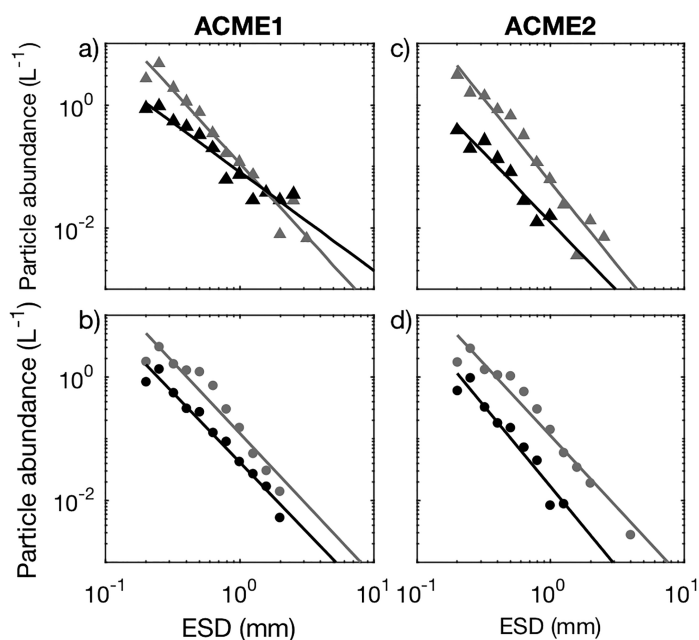


Fig. 7. Comparison of the slopes of the particle size spectrum in the 10 m depth interval above and below *Poeobius* sp. in ACME1 and ACME2, compared to the background (mean reference) conditions obtained during five cruises (12 profiles). ACME conditions are depicted in lines and triangles (**a**, **c**), background conditions in lines and points (**b**, **d**) with gray representing the shallow depth interval and black the deep depth interval, respectively.

Fig. 6e). Below 50 m, the calculated PARR in ACME1 was similar to background conditions. In ACME2, PARR was within the confidence interval of the background profiles above 100 m and below 300 m depth. PARR was significantly reduced at depths between 100 m and 300 m with minimum rates below $4 \mu\text{mol kg}^{-1} \text{yr}^{-1}$ (Fig. 6f). *Poeobius* sp. individual respiration rates ranged between $0.00028 \mu\text{mol h}^{-1}$ and $0.0064 \mu\text{mol h}^{-1}$ in ACME 1 and between $0.0084 \mu\text{mol h}^{-1}$ and $0.02 \mu\text{mol h}^{-1}$ in ACME2. Maximum community respiration calculated for *Poeobius* sp. was $0.84 \mu\text{mol kg}^{-1} \text{yr}^{-1}$ in ACME1 and $2.27 \mu\text{mol kg}^{-1} \text{yr}^{-1}$ in ACME2.

Particle size distribution

We compared the change in slope of the particle abundance spectrum from above to below the layer in which *Poeobius* sp. occurred in ACME1 and ACME2 and the respective background spectrum (Fig. 7). In ACME1, the slope of the particle spectrum of the deeper layer was shallower, leading to a crossing of slopes at around 1.5 mm particle size (Fig. 7a). This indicates reduced particle abundances in the layer below *Poeobius* sp. (compared to the shallow layer) mainly in the small size classes and partly elevated abundances in the larger size classes. In the background situation, the slopes were similar in both depth intervals and were almost parallel, indicating very little change in the particle size spectrum apart from a reduction in particle abundance with

depth (Fig. 7b). In ACME2, the difference in slopes between the shallow and the deep layer was only small, although a trend toward a shallower slope in the deeper layer of the ACME could be observed (Fig. 7c). In the background profiles at these depth intervals, the slope of the particle spectrum was rather larger than in the shallow interval, but here again the difference was only small (Fig. 7d).

Poeobius sp. flux interception potential

In order to estimate the potential impact of flux feeding on the downward particle flux, the area of *Poeobius* sp. mucous nets was measured on five PELAGIOS frame shots (Supporting Information Fig. S2, Video S1). The mean shape of mucous nets was irregular with lengths of about 9.9 (mean value; range = 8.5–11.2, SD = 1) and widths of approximately 1.7 times (mean value; range = 0.9–2.9, SD = 0.8) *Poeobius* sp. body length, respectively (Supporting Information Table S2). Mucous net areas approximated as prolate ellipse from net length and width (mean 12.7 cm^2 assuming a *Poeobius* sp. length of 1 cm, SD = 5.4 cm^2) were similar to the manually measured relative net area (mean 12.3 cm^2 , SD = 6.6 cm^2). We therefore established the following relationship to calculate mucous net area (A_{net} , m^2) from *Poeobius* sp. length (length_{poeo}, mm):

$$A_{\text{net}} = \frac{\pi \times \left(\frac{\text{length}_{\text{poeo}} \times 9.9}{2}\right) \times \left(\frac{\text{length}_{\text{poeo}} \times 1.7}{2}\right)}{1000} \quad (8)$$

Mucous nets were visible in about 40% of the *Poeobius* sp. on the selected PELAGIOS transects, but could only be identified when particles were attached to them which is why we only have five distinct measurements of mucous net size.

Within ACME1, we observed a *Poeobius* sp. standing stock of 5500 ind m^{-2} in a 30 m depth interval (45–75 m). Length measurements of all individuals observed yielded a mean length of 6.7 mm. The established length to mucous net area relationship (Eq. 8) allows us to calculate a mean individual mucous net area of about 6 cm^2 . Our PELAGIOS video observations reveal that approximately 40% of the *Poeobius* sp. standing stock have their mucous nets deployed. If we assume that their nets align perfectly, we can come to the conclusion that the mucous nets deployed by *Poeobius* sp. individuals in ACME1 cover an area of 1.3 m^2 per square meter in ACME1, yielding a 1.3-fold flux interception potential. In ACME2, *Poeobius* sp. of mean length 14 mm occurred in a 45 m depth interval (65–110 m) with a standing stock of 500 ind m^{-2} and with a mean individual net area of 26 cm^2 . With the same assumptions as above, this leads to a total covered area of 0.51 m^2 per square meter, i.e., about 50% flux interception potential in ACME2. Given that the mucous nets are unlikely to be perfectly aligned (i.e., without overlaps), the actually covered area was probably smaller. However, extended tentacles, which may also indicate active feeding (Uttal and Buck 1996), were visible in more than

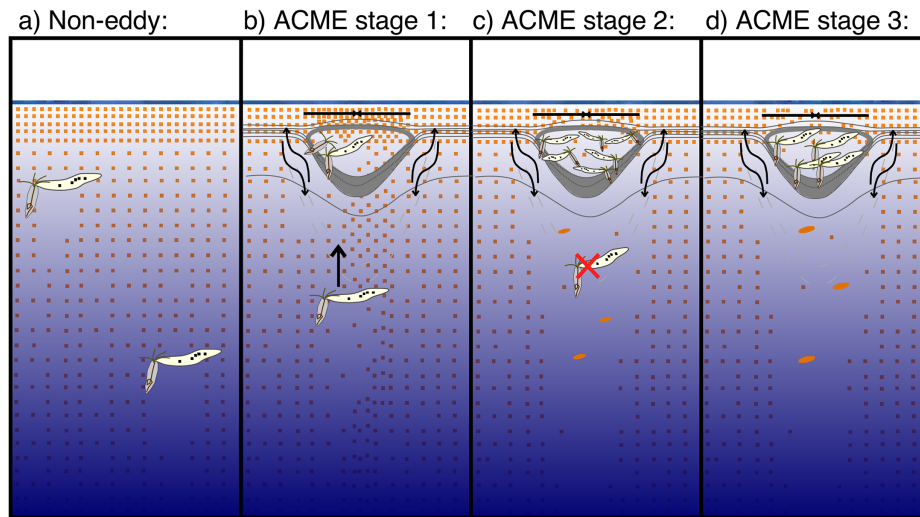


Fig. 8. Schematic illustrating the potential processes during the lifetime of an ACME if it becomes heavily colonized by *Poebobius* sp. Dots represent particles in the water column. **(a)** Non-eddy open ocean conditions: *Poebobius* sp. are evenly distributed in the upper 1000 m of the water column in low abundances. **(b)** *Poebobius* sp. aggregate in the ACME core, likely due to active vertical migration. Particle production is enhanced due to nutrient input into the euphotic zone and a high-quality food signal triggers upward migration of individuals into the eddy. Optimal feeding conditions and higher encounter rates facilitate reproduction of *Poebobius* sp. The isolation of the eddy core prohibits spreading of the polychaete into the ambient ocean. **(c)** Large numbers of *Poebobius* sp. compete for sinking particles—they aggregate close to the mixed layer. Low oxygen conditions in the eddy core exclude potential predators and competitors. Particle abundances are reduced as small particles are repackaged into fast sinking, large fecal pellets. **(d)** Reduced nutrient cycling results in low productivity in a later stage of the eddy. *Poebobius* sp. repackage the remaining flux in the ACME. Stage **(c)** represents the situation that was found in ACME1. ACME2 may have been an ACME of stage **(b)** or **(d)**. Eddy schematic modified from Karstensen et al. (2017).

80% of the observed *Poebobius* sp. specimens on PELAGIOS video transects, suggesting that the number of visible mucous nets likely underestimates the actual proportion of actively feeding *Poebobius* sp.

Discussion

Our analysis reveals that the flux feeder *Poebobius* sp. had significantly larger standing stocks in ACMEs, compared to ACs, CEs, and non-eddy open ocean conditions. We furthermore conclude that *Poebobius* sp. impacts the particle distribution and flux in ACMEs by feeding with their mucous nets. Here, we first discuss possible mechanisms that lead to the observed patterns and then relate to the potential biogeochemical impacts that flux feeding by *Poebobius* sp. can cause in ACMEs.

Increased *Poebobius* sp. abundances in mesoscale eddies

Several mechanisms or a combination thereof may explain the increased abundance of *Poebobius* sp. in ACMEs. These mechanisms include physical aggregation and advection, active habitat choice and improved survival and reproduction due to beneficial habitat conditions.

1. Physical aggregation and advection: ACME cores are strongly isolated and there is virtually no lateral exchange with surrounding waters, as shown by very stable temperature and salinity conditions in ACMEs over periods of several

months (Karstensen et al. 2015, 2017). It therefore seems unlikely that they collect zooplankton from the upper ~ 400 m of the surrounding ocean on their path. However, the isolation could result in an export of *Poebobius* sp. specimens from the coastal areas of the Mauritanian shelf region westward, into the open ocean (Schütte et al. 2016b). Nevertheless, our observations do not show an enhanced abundance of *Poebobius* sp. off Mauretania, lending no support to this hypothesis.

2. Active habitat choice: Enhanced abundances of zooplankton (Hauss et al. 2016) and nekton (Godø et al. 2012) near the surface of mesoscale eddies can result in increased flux of fecal pellets to depth (Goldthwait and Steinberg 2008) and may lead to an export of large quantities of fresh particulate matter down to the seafloor (Beaulieu 2002). Fecal pellets made up the majority of nutritious food items that were found in *P. meseres* stomachs (Uttal and Buck 1996) and may thus be perceived as “high-quality food” by the polychaetes. We hypothesize that *Poebobius* sp. migrate into the ACMEs from below approximately 400 m depth, triggered, for example, by the high-quality food signal that these eddies emit to the deep sea via enhanced particle flux while they travel. In non-eddy conditions, the integrated standing stock between 400 m and 1000 m depth from where individuals could migrate into the isolated eddy core, was about 10 ind m⁻², whereas in ACME1 and ACME2

between 0 m and 150 m depth, it was about 552- and 50-fold elevated (5523 ind m⁻² and 500 ind m⁻², respectively). It follows that, with a diameter of about 100 km, and neglecting population dynamical processes such as reproduction, ACME1 would have needed to travel about 55,230 km and ACME2 5000 km in order to “collect” the observed *Poeobius* sp. Eddies in the area generally originate at the African coast at about 600–1000 km distance from the 23°W section. Active habitat choice can therefore not explain the especially large stocks in ACME1 and ACME2, even if all *Poeobius* sp. on the eddies’ path migrated into the eddy. However, a probable path of 600–1000 km may lead to a 6- to 10-fold increase in abundance which might already be important for further population dynamical processes in the eddy.

Additionally, the strong upward shift in the depth distribution of *Poeobius* sp. in ACMEs could be a result of active habitat choice, likely amplified by intraspecific competition for space and food, as already outlined by Jackson (1993) for pteropods. Low abundances of flux feeders, as found in non-eddy open ocean conditions, result in a low total cross-sectional area of mucous nets (\sum_{netarea}) that only weakly attenuates flux with depth, providing no reason to compete for space in a certain depth layer (Fig. 8a). In contrast, if abundances increase, e.g., due to active migration into favorable conditions (Fig. 8b), a high \sum_{netarea} leaves only a small fraction of the near-surface flux to settle into deeper layers. We calculated that *Poeobius* sp. could potentially intercept all of the gravitational flux in ACME1 and 50% in ACME2. Such strong flux attenuation might lead to a strategy where flux-feeders gather directly below their food source, which may explain the strongly condensed depth distribution that we observed in ACMEs with high *Poeobius* sp. abundances (Fig. 8c,d).

3. Increased survival and reproduction due to beneficial conditions: *Poeobius* sp. has separate sexes and an external fertilization (Robbins 1965). Higher encounter rates in eddies due to active habitat choice and a resulting “concentration effect” may facilitate reproduction. In order to assess the potential reproduction of *Poeobius* sp. in the observed eddies, we would need information such as their egg numbers, development time, and growth rates. However, an intensive literature search did not reveal any such information. Short life cycles and the capability to form blooms as a response to environmental triggers are however a well-known feature of gelatinous zooplankton (e.g., Boero et al. 2008). Maximum ACME lifetimes of about 200 d (Schütte et al. 2016b) should allow for reproduction and larval development also for sexually reproducing invertebrates such as *Poeobius* sp. The highest recorded abundance of *Poeobius* sp. in ACME1 coincided with the smallest mean size of the individual polychaetes, which in our view points to a recent reproduction event.

In addition to increasing the likelihood of reproduction due to a “concentration effect,” ACMEs probably also

improve the survival of *Poeobius* sp. ACMEs generally provide beneficial growth conditions for flux-feeders as ACME cores are low mixing regions (Karstensen et al. 2017) where fragile mucous nets are well preserved and feeding is not disrupted by turbulence (Tsurumi et al. 2005). Furthermore, generally elevated particle loads in ACMEs and CEs (Sweeney et al. 2003; Fiedler et al. 2016; Hauss et al. 2016) provide beneficial conditions for the growth of flux-feeding organisms. However, near-surface particle concentrations in ACME1 and ACME2 were not particularly enhanced, and in ACME2 even lower than the background signal. One explanation for this could be that eddy productivity is episodic (Karstensen et al. 2017). Especially in later stages of their lifetime, particle production in ACMEs may not differ from the background (Buesseler et al. 2008), although it was probably high during earlier stages. Reduced oxygen concentrations in both eddies, and especially in ACME1, indicate strong oxygen consumption, possibly generated by a high particle load and remineralization during the earlier isolation time of the eddies (Buesseler et al. 2008). These low oxygen concentrations may also be beneficial to the survival of *Poeobius* sp. Oxygen concentrations were below 20 $\mu\text{mol kg}^{-1}$ in ACME1 and *Poeobius* sp. dominated the zooplankton community (about 50% contribution) at these oxygen levels. These levels are below the critical physiological threshold for some competitors like copepods (Kiko et al. 2016) and pteropods (Maas et al. 2012), as well as for potential predators such as squid and fish (Purcell and Arai 2001; Seibel 2011; Cardona et al. 2012). Some gelatinous predators may however tolerate these low oxygen concentrations (Purcell et al. 2001). In ACME2, on the other hand, oxygen concentrations did not drop below 45 $\mu\text{mol kg}^{-1}$ and should therefore not exclude competitors and predators. These considerations are supported by the observation of some krill and copepods, as well as large siphonophores in a pelagic video transect in ACME2. However, the numbers of these zooplankton organisms were considerably lower than those of *Poeobius* sp.

Summarizing the discussion of enhanced abundances of *Poeobius* sp. in ACMEs, we suggest that active habitat choice as well as increased survival and reproduction may have contributed to the enhanced abundance of *Poeobius* sp. in ACMEs. Especially high particle fluxes and, through exclusion of predators and competitors, low oxygen concentrations seem to generate a unique niche that favors growth, reproduction, and survival of this species. Similar conditions may be found in upwelling areas such as the Monterey Canyon where *P. meseres* is highly abundant (Robison et al. 2010). Also, the encounter rate of these organisms is enhanced in mesoscale eddies in comparison to the open ocean which might be important for their reproductive success. The large standing stock of small individuals in ACME1 is probably the result of a relatively recent reproduction event. These findings underline the potential importance of

mesoscale eddies for the survival and dispersion of rare zooplankton species and support theoretical studies that see mesoscale eddies as a solution to the paradox of the plankton (Bracco et al. 2000).

Potential influences of *Poeobius* sp. on particle distribution and flux

Increased abundances of *Poeobius* sp. in ACME1 and ACME2 at shallow depth co-occurred with reduced particle abundances, especially in ACME2. The almost complete absence of particles between 110 m and 210 m in ACME2 is unique in our current dataset of 177 UVP5 profiles in the region (between 5–10°N and 25–20°W).

We observed a relatively high stratification in ACME1 and ACME2 compared to the background conditions. Sharp density gradients, especially when due to strong increases in salinity, can slow down sinking particles at the pycnocline (MacIntyre et al. 1995; Kindler et al. 2010). This can lead to a peak in the particle abundance profile and a reduced transport of particles into deeper layers, if these peaks are hot-spots of particle remineralization (MacIntyre et al. 1995). We would thus expect an accumulation of particles at the pycnocline of the ACMEs and a reduction in particle abundance below. In ACME1, a significant particle peak was observed just below the pycnocline and coincided with *Poeobius* sp. occurrence, possibly due to beneficial feeding conditions. Particle abundances were within background range below the peak, which indicates a stronger reduction of particle abundances than in background conditions. In ACME2, particle abundances were not elevated at the pycnocline. Particle abundances were normal just below the pycnocline, where *Poeobius* sp. occurred, but were significantly reduced below the polychaetes. We therefore consider that the particularly strong reduction of particle abundances in ACME1 might result from particle retention at the pycnocline and *Poeobius* sp. flux feeding, and in ACME2 almost exclusively from *Poeobius* sp. flux feeding.

We calculated a 1.3-fold and 0.5-fold coverage potential of the water column by *Poeobius* sp. mucous nets in ACME1 and ACME2, respectively. This result and the observation that *Poeobius* sp. dominated the zooplankton community in the respective layers of both eddies is in our view another clear indication that *Poeobius* sp. has substantially contributed to the particle depletion and thus had a strong influence on the biogeochemistry of the eddy.

Biogeochemical consequences of flux feeding

Substantial flux feeding can have different consequences for eddy oxygen concentration and nutrient cycling:

1. Enhancement of remineralization and respiration by flux attenuation: By intercepting the particle flux, *Poeobius* sp. could possibly enhance remineralization and respiration at the depth where they feed. This would lead to an intensification of the oxygen minimum zone in the eddy and

to a reduction of carbon export to deeper layers. However, the maximum *Poeobius* sp. community respiration of 2.27 $\mu\text{mol kg}^{-1} \text{yr}^{-1}$, observed in ACME2, would take about 24 yr to create an oxygen deficit of 55 $\mu\text{mol kg}^{-1}$. Such a deficit results if we assume an oxygen concentration of $\sim 75 \mu\text{mol kg}^{-1}$ at eddy formation (value for Mauritanian shelf concentrations; Fiedler et al. 2016) and subtract the observed concentration of about 20 $\mu\text{mol kg}^{-1}$ between 60 m and 70 m depth during the sampling of ACME1. As ACMEs in the area have lifetimes below 7 months (Schütte et al. 2016b), it follows that the oxygen deficit must be the result of zooplankton and particle dynamics at an earlier stage of the eddy. Mucous nets collect microzooplankton (Gilmer 1972) and microbes associated with sinking particles which may lead to enhanced local biological activity and respiration. However, as they are ingested regularly, it seems unlikely that they massively support microbial growth and respiration.

2. Particle repackaging and generation of a deep penetrating flux: Considering the very low community respiration rates of *Poeobius* sp. (maximum 2.27 $\mu\text{mol kg}^{-1} \text{yr}^{-1}$), we suggest that it is more likely that, rather than assimilating the captured particles efficiently, *Poeobius* sp. collect sinking particles and repackage them into larger, rapidly sinking, fecal pellets (as described for salps; e.g., Madin 1982). Through this process they would reduce particle associated remineralization and respiration at their feeding depth. Uttal and Buck (1996) described *P. meseres* fecal pellets to “appear watery and remain intact” after egestion in the laboratory. However, settling experiments and observations of *P. meseres* fecal pellets (B. Robison and R. Sherlock unpubl.) in Monterey Bay indicate that the fecal pellet morphology, consistency, and sinking velocity can vary considerably, probably depending on the type of ingested food and feeding technique. Some fecal pellets were watery and very fragile, but some also compact and dense. An assessment of sinking rates resulted in a median sinking speed of 175 m d^{-1} (range 35–869 m d^{-1}). The maximum sinking speed of 869 m d^{-1} suggests that a rapid carbon export by *Poeobius* sp. fecal pellets is feasible. Analysis of the size spectrum slope above and below the occurrence of *Poeobius* sp. also indicates a reduction of small particles in ACME1 and ACME2 and partly even an increase in larger particles below the depth where *Poeobius* sp. occurred. These observations further support our hypothesis that the polychaetes repackage small particles into larger, more rapidly sinking fecal pellets. It is probably due to the very low productivity of ACME2 that this pattern was less obvious in this eddy, i.e., input particle abundances may have been too low to generate an increased output flux in comparison to the background situation.

The removal of particles from the core of ACMEs by *Poeobius* sp. suggests a strong impact on the biogeochemistry and

the pathway of carbon in the water column. In addition to reducing the direct remineralization of particles—as indicated by reduced microbial particle associated respiration rates at midwater depth—the proposed deep penetrating flux could also result in a loss of nutrients from the eddy: Karstensen et al. (2017) described an “outward directed mixing” or “erosion” of the ACME core because the low-mixing core is surrounded by regions of strong mixing. They relate the erosion to upwelling processes and conclude that by this upwelling and by eddy retention, dissolved nutrients such as NO_3^- are transported from the margins of the eddy core back into the euphotic zone of the eddy where they can be utilized by autotrophs and later are reintroduced into the eddy core in the form of sinking particulate matter. If the particulate matter that reaches the eddy core is not remineralized but instead directly exported into deeper layers—e.g., via repackaging by *Poeobius* sp.—this recycling process is weakened and less nutrients are made available for surface productivity. This may explain the low near-surface particle concentrations of ACME1 and ACME2 compared to other ACMEs (Fiedler et al. 2016). The generation of a deep penetrating flux could also—in contrast to consequence 1—attenuate oxygen consumption in eddies and could prevent eddies from turning anoxic as particle removal reduces substrate for microbial respiration.

Conclusion

Based on our findings, we developed a conceptual model for the evolution of a *Poeobius* sp. aggregation inside eddies (Fig. 8). We suggest that the high abundance of *Poeobius* sp. in ACMEs compared to non-eddy conditions is the result of the combination of an accumulating effect by active vertical migration into the eddy and improved survival and reproduction in ACME conditions. *Poeobius* sp. appears to benefit from enhanced particle fluxes in ACMEs and potentially from the exclusion of hypoxia intolerant competitors and predators. This indicates that mesoscale eddies can serve as an important niche for marine biodiversity by aggregating otherwise low-abundant species. The shallow and narrow depth distribution of *Poeobius* sp. in ACMEs is probably a result of both the competition of the flux-feeding animals for sinking particles and the physical isolation of the eddy core. Very low particle concentrations and a change in the particle size distribution were measured below layers with high *Poeobius* sp. abundances and our analysis suggests that the polychaete worms were the ultimate cause for these particularly low particle numbers. However, seemingly stochastic heterogeneity of *Poeobius* sp. abundance in different eddies still makes it difficult to assess the large-scale impacts of *Poeobius* sp. on eddy biogeochemistry in general. Our work nevertheless underlines that not only physical and microbial processes, but even individual, fragile zooplankton species may substantially affect biogeochemical processes in the open ocean.

References

- Allredge, A. 1998. The carbon, nitrogen and mass content of marine snow as a function of aggregate size. *Deep-Sea Res. Part I Oceanogr. Res. Pap.* **45**: 529–541. doi:10.1016/S0967-0637(97)00048-4
- Angel, M. V. 1984. Detrital organic fluxes through pelagic ecosystems, p. 475–516. *In* M. J. R. Fasham [ed.], *Flows of energy and materials in marine ecosystems*. Springer.
- Beaulieu, S. E. 2002. Accumulation and fate of phytodetritus on the sea floor, p. 171–232. *In* R. N. Gibson and M. Barnes [eds.], *Oceanography and marine biology: An annual review*. Taylor & Francis.
- Bianchi, D., E. D. Galbraith, D. A. Carozza, K. A. S. Mislán, and C. A. Stock. 2013. Intensification of open-ocean oxygen depletion by vertically migrating animals. *Nat. Geosci.* **6**: 545–548. doi:10.1038/ngeo1837
- Biard, T., and others. 2016. In situ imaging reveals the biomass of giant protists in the global ocean. *Nature* **532**: 504–507. doi:10.1038/nature17652
- Boero, F., J. Bouillon, C. Gravili, M. P. Miglietta, T. Parsons, and S. Piraino. 2008. Gelatinous plankton: Irregularities rule the world (sometimes). *Mar. Ecol. Prog. Ser.* **356**: 299–310. doi:10.3354/meps07368
- Bracco, A., A. Provenzale, and I. Scheuring. 2000. Mesoscale vortices and the paradox of the plankton. *Proc. R. Soc. B Biol. Sci.* **267**: 1795–1800. doi:10.1098/rspb.2000.1212
- Brandt, P., and others. 2015. On the role of circulation and mixing in the ventilation of oxygen minimum zones with a focus on the eastern tropical North Atlantic. *Biogeosciences* **12**: 489–512. doi:10.5194/bg-12-489-2015
- Buesseler, K. O., and others. 2008. Particle fluxes associated with mesoscale eddies in the Sargasso Sea. *Deep-Sea Res. Part II Top. Stud. Oceanogr.* **55**: 1426–1444. doi:10.1016/j.dsr2.2008.02.007
- Cardona, L., I. Álvarez de Quevedo, A. Borrell, and A. Aguilar. 2012. Massive consumption of gelatinous plankton by mediterranean apex predators. *PLoS One* **7**: e31329–e31314. doi:10.1371/journal.pone.0031329
- Cavan, E. L., S. A. Henson, A. Belcher, and R. Sanders. 2017. Role of zooplankton in determining the efficiency of the biological carbon pump. *Biogeosciences* **14**: 177–186. doi:10.5194/bg-14-177-2017
- Chelton, D. B., M. G. Schlax, and R. M. Samelson. 2011. Global observations of nonlinear mesoscale eddies. *Prog. Oceanogr.* **91**: 167–216. doi:10.1016/j.pocean.2011.01.002
- Fiedler, B., and others. 2016. Oxygen utilization and downward carbon flux in an oxygen-depleted eddy in the eastern tropical North Atlantic. *Biogeosciences* **13**: 5633–5647. doi:10.5194/bg-13-5633-2016
- Field, C. B., M. J. Behrenfeld, J. T. Randerson, and P. Falkowski. 1998. Primary production of the biosphere: Integrating terrestrial and oceanic components. *Science* **281**: 237–240. doi:10.1126/science.281.5374.237

- Frangoulis, C., N. Skliris, G. Lepoint, K. Elkalay, A. Goffart, J. K. Pinnegar, and J.-H. Hecq. 2011. Importance of copepod carcasses versus faecal pellets in the upper water column of an oligotrophic area. *Estuar. Coast. Shelf Sci.* **92**: 456–463. doi:10.1016/j.ecss.2011.02.005
- Gilmer, R. W. 1972. Free-floating mucus webs: A novel feeding adaptation for the open ocean. *Science* **176**: 1239–1240. doi:10.1126/science.176.4040.1239
- Godø, O. R., A. Samuelsen, G. J. Macaulay, R. Patel, S. S. Hjøllø, J. Horne, S. Kaartvedt, and J. A. Johannessen. 2012. Mesoscale eddies are oases for higher trophic marine life. *PLoS One* **7**: e30161–e30169. doi:10.1371/journal.pone.0030161
- Goldthwait, S. A., and D. K. Steinberg. 2008. Elevated biomass of mesozooplankton and enhanced fecal pellet flux in cyclonic and mode-water eddies in the Sargasso Sea. *Deep-Sea Res. Part II Top. Stud. Oceanogr.* **55**: 1360–1377. doi:10.1016/j.dsr2.2008.01.003
- Hamner, W. M., L. P. Madin, A. L. Alldredge, R. W. Gilmer, and P. P. Hamner. 1975. Underwater observations of gelatinous zooplankton: Sampling problems, feeding biology, and behavior. *Limnol. Oceanogr.* **20**: 907–917. doi:10.4319/lo.1975.20.6.0907
- Hauss, H., and others. 2016. Dead zone or oasis in the open ocean? Zooplankton distribution and migration in low-oxygen modewater eddies. *Biogeosciences* **13**: 1977–1989. doi:10.5194/bg-13-1977-2016
- Heath, H. 1930. A connecting link between the Annelida and the Echiuroidea (*Gephyrea armata*). *J. Morphol.* **49**: 223–249. doi:10.1002/jmor.1050490106
- Heinze, C., S. Meyer, N. Goris, L. Anderson, R. Steinfeldt, N. Chang, C. Le Quéré, and D. C. E. Bakker. 2015. The ocean carbon sink – impacts, vulnerabilities and challenges. *Earth Syst. Dyn.* **6**: 327–358. doi:10.5194/esd-6-327-2015
- Iversen, M. H., N. Nowald, H. Ploug, G. A. Jackson, and G. Fischer. 2010. High resolution profiles of vertical particulate organic matter export off Cape Blanc, Mauritania Degradation processes and ballasting effects. *Deep-Sea Res. Part I Oceanogr. Res. Pap.* **57**: 771–784. doi:10.1016/j.dsr.2010.03.007
- Jackson, G. A. 1993. Flux feeding as a mechanism for zooplankton grazing and its implications for vertical particulate flux. *Limnol. Oceanogr.* **38**: 1328–1331. doi:10.4319/lo.1993.38.6.1328
- Jia, Y., E. Shelhamer, J. Donahue, S. Karayev, J. Long, R. Girshick, S. Guadarrama, and T. Darrel. 2014. Caffe: Convolutional architecture for fast feature embedding, p. 675–678. *In Proceedings of the ACM International Conference on Multimedia - MM '14*, Orlando, Florida, USA—November 03–07, 2014. V. 978. doi:10.1145/2647868.2654889
- Jiao, N., and others. 2010. Microbial production of recalcitrant dissolved organic matter: Long-term carbon storage in the global ocean. *Nat. Rev. Microbiol.* **8**: 593–599. doi:10.1038/nrmicro2386
- Kalvelage, T., and others. 2015. Aerobic microbial respiration in oceanic oxygen minimum zones. *PLoS One* **10**: e0133526. doi:10.1371/journal.pone.0133526
- Karstensen, J., L. Stramma, and M. Visbeck. 2008. Oxygen minimum zones in the eastern tropical Atlantic and Pacific oceans. *Prog. Oceanogr.* **77**: 331–350. doi:10.1016/j.pocean.2007.05.009
- Karstensen, J., and others. 2015. Open ocean dead zones in the tropical North Atlantic Ocean. *Biogeosciences* **12**: 2597–2605. doi:10.5194/bg-12-2597-2015
- Karstensen, J., and others. 2017. Upwelling and isolation in oxygen-depleted anticyclonic modewater eddies and implications for nitrate cycling. *Biogeosciences* **14**: 2167–2181. doi:10.5194/bg-14-2167-2017
- Kiko, R., H. Hauss, F. Buchholz, and F. Melzner. 2016. Ammonium excretion and oxygen respiration of tropical copepods and euphausiids exposed to oxygen minimum zone conditions. *Biogeosciences* **13**: 2241–2255. doi:10.5194/bg-13-2241-2016
- Kindler, K., A. Khalili, and R. Stocker. 2010. Diffusion-limited retention of porous particles at density interfaces. *Proc. Natl. Acad. Sci. USA* **107**: 22163–22168. doi:10.1073/pnas.1012319108
- Kjørboe, T. 2000. Colonization of marine snow aggregates by invertebrate zooplankton: Abundance, scaling, and possible role. *Limnol. Oceanogr.* **45**: 479–484. doi:10.4319/lo.2000.45.2.0479
- Kriest, I. 2002. Different parameterizations of marine snow in a 1D-model and their influence on representation of marine snow, nitrogen budget and sedimentation. *Deep-Sea Res. Part I Oceanogr. Res. Pap.* **49**: 2133–2162. doi:10.1016/s0967-0637(02)00127-9
- LeCun, Y., Y. Bengio, and G. Hinton. 2015. Deep learning. *Nature* **521**: 436–444. doi:10.1038/nature14539
- Legendre, L., and R. B. Rivkin. 2002. Fluxes of carbon in the upper ocean: Regulation by food-web control nodes. *Mar. Ecol. Prog. Ser.* **242**: 95–109. doi:10.3354/meps242095
- Lehette, P., and S. Hernández-León. 2009. Zooplankton biomass estimation from digitized images: A comparison between subtropical and Antarctic organisms. *Limnol. Oceanogr.: Methods* **7**: 304–308. doi:10.4319/lom.2009.7.304
- Lévy, M., R. Ferrari, P. J. S. Franks, A. P. Martin, and P. Rivière. 2012. Bringing physics to life at the submesoscale. *Geophys. Res. Lett.* **39**: L14602. doi:10.1029/2012gl052756
- Longhurst, A. R., A. W. Bedo, W. G. Harrison, E. J. H. Head, and D. D. Sameoto. 1990. Vertical flux of respiratory carbon by oceanic diel migrant biota. *Deep-Sea Res. Part A Oceanogr. Res. Pap.* **37**: 685–694. doi:10.1016/0198-0149(90)90098-G
- Löscher, C. R., and others. 2015. Hidden biosphere in an oxygen-deficient Atlantic open-ocean eddy: Future implications of ocean deoxygenation on primary production in the eastern tropical North Atlantic. *Biogeosciences* **12**: 7467–7482. doi:10.5194/bg-12-7467-2015

- Maas, A. E., K. F. Wishner, and B. A. Seibel. 2012. Metabolic suppression in thecosomatous pteropods as an effect of low temperature and hypoxia in the eastern tropical North Pacific. *Mar. Biol.* **159**: 1955–1967. doi:10.1007/s00227-012-1982-x
- MacIntyre, S., A. L. Alldredge, and C. C. Gotschalk. 1995. Accumulation of marines now at density discontinuities in the water column. *Limnol. Oceanogr.* **40**: 449–468. doi:10.4319/lo.1995.40.3.0449
- Madin, L. P. 1982. Production, composition and sedimentation of salp fecal pellets in oceanic waters. *Mar. Biol.* **67**: 39–45. doi:10.1007/bf00397092
- McDonnell, A. M. P., and K. O. Buesseler. 2012. A new method for the estimation of sinking particle fluxes from measurements of the particle size distribution, average sinking velocity, and carbon content. *Limnol. Oceanogr.: Methods* **10**: 329–346. doi:10.4319/lom.2012.10.329
- McDougall, T., and P. M. Barker. 2015. Getting started with TEOS-10 and the Gibbs Seawater (GSW) Oceanographic Toolbox, 28 pp., SCOR/IAPSO WG127.
- McGillicuddy, D. J., and others. 2007. Eddy/wind interactions stimulate extraordinary mid-ocean plankton blooms. *Science* **316**: 1021–1026. doi:10.1126/science.1136256
- McGowan, J. A. 1959. The relationship of the distribution of the planktonic worm, *Poeobius meseres* Heath, to the water masses of the North Pacific. *Deep-Sea Res.* **6**: 125–139. doi:10.1016/0146-6313(59)90064-4
- d'Ovidio, F., S. De Monte, A. Della Penna, C. Cotté, and C. Guinet. 2013. Ecological implications of eddy retention in the open ocean: A Lagrangian approach. *J. Phys. A Math. Theor.* **46**: 254023. doi:10.1088/1751-8113/46/25/254023
- Packard, T. T., and M. Gómez. 2013. Modeling vertical carbon flux from zooplankton respiration. *Prog. Oceanogr.* **110**: 59–68. doi:10.1016/j.pocean.2013.01.003
- Picheral, M., L. Guidi, L. Stemmann, D. M. Karl, G. Iddaoud, and G. Gorsky. 2010. The Underwater Vision Profiler 5: An advanced instrument for high spatial resolution studies of particle size spectra and zooplankton. *Limnol. Oceanogr.: Methods* **8**: 462–473. doi:10.4319/lom.2010.8.462
- Ploug, H., M. Kühl, B. Buchholz-Cleven, and B. B. Jørgensen. 1997. Anoxic aggregates—an ephemeral phenomenon in the pelagic environment? *Aquat. Microb. Ecol.* **13**: 285–294. doi:10.3354/ame013285
- Purcell, J. E., and M. N. Arai. 2001. Interactions of pelagic cnidarians and ctenophores with fish: A review. *Hydrobiologia* **451**: 27–44. doi:10.1007/978-94-010-0722-1_4
- Purcell, J. E., D. L. Breitburg, M. B. Decker, W. M. Graham, M. J. Youngbluth, and K. A. Raskoff. 2001. Pelagic cnidarians and ctenophores in low dissolved oxygen environments: A review, p. 77–100. *In* N. N. Rabalais and R. E. Turner [eds.], *Coastal hypoxia: Consequences for living resources and ecosystems*. American Geophysical Union.
- Redfield, A. C., B. H. Ketchum, and F. A. Richards. 1963. The influence of organisms on the composition of sea-water, p. 26–77. *In* M. N. Hill [ed.], *The composition of seawater: Comparative and descriptive oceanography. The sea: Ideas and observations on progress in the study of the seas*. V. 2. Wiley Interscience.
- Riley, G. A. 1951. Oxygen, phosphate, and nitrate in the Atlantic Ocean. *Bulletin of the Bingham Oceanographic Collection* **13**: 1–126.
- Ring, G. 1981. Gulf stream cold-core rings: Their physics, chemistry, and biology. *Science* **212**: 1091–1100. doi:10.1126/science.212.4499.1091
- Robbins, D. E. 1965. The biology and morphology of the pelagic annelid *Poeobius meseres* Heath. *J. Zool.* **146**: 197–212. doi:10.1111/j.1469-7998.1965.tb05209.x
- Robison, B. H., R. E. Sherlock, and K. R. Reisenbichler. 2010. The bathypelagic community of Monterey Canyon. *Deep-Sea Res. Part II Top. Stud. Oceanogr.* **57**: 1551–1556. doi:10.1016/j.dsr2.2010.02.021
- Sabine, C. L., and T. Tanhua. 2010. Estimation of anthropogenic CO₂ inventories in the ocean. *Ann. Rev. Mar. Sci.* **2**: 175–198. doi:10.1146/annurev-marine-120308-080947
- Schütte, F., J. Karstensen, G. Krahnemann, H. Hauss, B. Fiedler, P. Brandt, M. Visbeck, and A. Körtzinger. 2016a. Characterization of “dead-zone” eddies in the tropical Northeast Atlantic Ocean. *Biogeosciences* **13**: 5865–5881. doi:10.5194/bg-13-5865-2016
- Schütte, F., P. Brandt, and J. Karstensen. 2016b. Occurrence and characteristics of mesoscale eddies in the tropical northeastern Atlantic Ocean. *Ocean Sci.* **12**: 663–685. doi:10.5194/os-12-663-2016
- Seibel, B. A. 2011. Critical oxygen levels and metabolic suppression in oceanic oxygen minimum zones. *J. Exp. Biol.* **214**: 326–336. doi:10.1242/jeb.049171
- Steinberg, D. K., B. A. S. Van Mooy, K. O. Buesseler, P. W. Boyd, T. Kobari, and D. M. Karl. 2008. Bacterial vs. zooplankton control of sinking particle flux in the ocean's twilight zone. *Limnol. Oceanogr.* **53**: 1327–1338. doi:10.4319/lo.2008.53.4.1327
- Stemmann, L., G. A. Jackson, and G. Gorsky. 2004. A vertical model of particle size distributions and fluxes in the mid-water column that includes biological and physical processes—part II: Application to a three year survey in the NW Mediterranean Sea. *Deep-Sea Res. Part I Oceanogr. Res. Pap.* **51**: 885–908. doi:10.1016/j.dsr.2004.03.002
- Stemmann, L., A. Hosia, M. J. Youngbluth, H. Søiland, M. Picheral, and G. Gorsky. 2008. Vertical distribution (0–1000 m) of macrozooplankton, estimated using the Underwater Video Profiler, in different hydrographic regimes along the northern portion of the Mid-Atlantic Ridge. *Deep-Sea Res. Part II Top. Stud. Oceanogr.* **55**: 94–105. doi:10.1016/j.dsr2.2007.09.019
- Stramma, L., H. W. Bange, R. Czeschel, A. Lorenzo, and M. Frank. 2013. On the role of mesoscale eddies for the

- biological productivity and biogeochemistry in the eastern tropical Pacific Ocean off Peru. *Biogeosciences* **10**: 7293–7306. doi:10.5194/bg-10-7293-2013
- Sweeney, E. N., D. J. McGillicuddy, Jr., and K. O. Buesseler. 2003. Biogeochemical impacts due to mesoscale eddy activity in the Sargasso Sea as measured at the Bermuda Atlantic Time-series Study (BATS). *Deep-Sea Res. Part II Top. Stud. Oceanogr.* **50**: 3017–3039. doi:10.1016/j.dsr2.2003.07.008
- Thuesen, E. V., and J. J. Childress. 1993. Metabolic rates, enzyme activities and chemical compositions of some deep-sea pelagic worms, particularly *Nectonemertes mirabilis* (Nemertea; Hoplonemertinea) and *Poeobius meseres* (Annelida; Polychaeta). *Deep-Sea Res. Part I Oceanogr. Res. Pap.* **40**: 937–951. doi:10.1016/0967-0637(93)90082-E
- Tsurumi, M., D. L. Mackas, F. A. Whitney, C. DiBacco, M. D. Galbraith, and C. S. Wong. 2005. Pteropods, eddies, carbon flux, and climate variability in the Alaska Gyre. *Deep-Sea Res. Part II Top. Stud. Oceanogr.* **52**: 1037–1053. doi:10.1016/j.dsr2.2005.02.005
- Turner, J. T. 2015. Zooplankton fecal pellets, marine snow, phytodetritus and the ocean's biological pump. *Prog. Oceanogr.* **130**: 205–248. doi:10.1016/j.pocean.2014.08.005
- Uttal, L., and K. R. Buck. 1996. Dietary study of the mid-water polychaete *Poeobius meseres* in Monterey Bay, California. *Mar. Biol.* **125**: 333–343. doi:10.1007/BF00346314
- Volk, T., and M. I. Hoffert. 1985. Ocean carbon pumps: Analysis of relative strengths and efficiencies in ocean-driven atmospheric CO₂ changes. American Geophysical Union.
- Waite, A. M., and others. 2016. Cross-shelf transport, oxygen depletion, and nitrate release within a forming mesoscale eddy in the eastern Indian Ocean. *Limnol. Oceanogr.* **61**: 103–121. doi:10.1002/lno.10218
- Wilson, S. E., H. A. Ruhl, and K. L. Smith, Jr. 2013. Zooplankton fecal pellet flux in the abyssal northeast Pacific: A 15 year time-series study. *Limnol. Oceanogr.* **58**: 881–892. doi:10.4319/lo.2013.58.3.0881

Acknowledgments

We would like to thank Rob Sherlock for collecting *Poeobius meseres* fecal pellets, for the conduction of sinking rate measurements, and for valuable information about this polychaete. We also thank Kyra Schlining for her help with the PELAGIOS video material. We greatly appreciate the comments and suggestions of two anonymous reviewers. AK, FS, HH, JK, PB, and RK were supported by the Deutsche Forschungsgemeinschaft (DFG) as part of the Collaborative Research Centre (SFB) 754 "Climate-Biogeochemistry Interactions in the Tropical Ocean." RK and SC were furthermore supported by grant CP1650 and HJTH by grant CP1218 of the Cluster of Excellence 80 "Future Ocean." "The Future Ocean" is funded within the framework of the Excellence Initiative by the Deutsche Forschungsgemeinschaft (DFG) on behalf of the German federal and state governments. LS was supported by the Chair Vision by the CNRS/UPMC. Shiptime on RV *Meteor* and RV *Maria S. Merian* and supporting funds were provided by the DFG. We are grateful for the support of the chief scientists and crews onboard RV *Meteor*, RV *Maria S. Merian*, and RV *Isländia*. Pieter Vandromme supported the project in the very early phase and identified *Poeobius* sp. on the UVP5 images.

Conflict of Interest

None declared.

Submitted 21 September 2017

Revised 28 February 2018

Accepted 09 April 2018

Associate editor: Thomas Kjørboe